Successive instabilities of confined Leidenfrost puddles

2015 EPL 112 26002

(http://iopscience.iop.org/0295-5075/112/2/26002)

A Letters Journal Exploring the Frontiers of Physics

October 2015

EPL, **112** (2015) 26002
doi: 10.1209/0295-5075/112/26002

www.epljournal.org

Successive instabilities of confined Leidenfrost puddles

Pascal S. Raux, Guillaume Dupeux, Christophe Clanet and David Quéré

PMMH, UMR 7636, ESPCI - 75005 Paris, France
LadHyX, UMR 7646 École polytechnique - 91128 Palaiseau, France

received 24 July 2015; accepted in final form 14 October 2015
published online 5 November 2015

PACS 68.03.Cd – Surface tension and related phenomena
PACS 68.03.Fg – Evaporation and condensation of liquids
PACS 47.55.D- – Drops and bubbles

Abstract – A Leidenfrost drop confined between two hot plates is unstable, if large enough. After a short delay to build a central vapor pocket, it forms a ring which rapidly expands and eventually bursts. We analyze this sequence of instabilities theoretically, and show that the ring size increases in a non-linear manner as a function of time, in agreement with experiments.

Introduction. – Volatile liquids on sufficiently hot plates are in the Leidenfrost state, levitating on a cushion of their own vapor. Hence any change in atmospheric pressure [1], substrate shape [2] or textures at its surface [3–6] impacts the stability and behavior of Leidenfrost drops. On smooth, flat surfaces, these drops are in a fully non-wetting situation, and they do not boil because of the absence of contact with the substrate. However, when poured at a larger scale (centimetric, instead of millimetric), liquids exhibit a kind of bubbling behavior, since one chimney (or several, for even larger drops) appears across the liquid, resulting from the rise of the subjacent vapor [7–9].

Confining a Leidenfrost drop between two plates (in a Hele-Shaw cell) promotes evaporation since vapor cushions are then expected on both sides of the liquid [10]. It also allows a better control of the geometry of the drop, the thickness of the drop being no longer set by the capillary length. Here we show that after some delay, a confined puddle evolves into a liquid ring which grows, before spliting in disconnected droplets whose size is fixed by the degree of confinement. While it has been suggested that Leidenfrost drops could be used in microfluidics devices [1], the instability studied here limits the maximum size of Leidenfrost liquids that one can confine. More generally, this experiment confirms that these drops have original behaviors compared to other non-wetting drops, owing to the production of vapor [2,6]. A study of Raufaste *et al.* [11], simultaneous to the present work, also focused on this instability. As those authors injected liquid directly inside the Hele-Shaw cell until a ring forms, drops then are always at the onset of instability. We propose here a slightly different set-up, allowing us to vary the size of the drop for a given confinement.

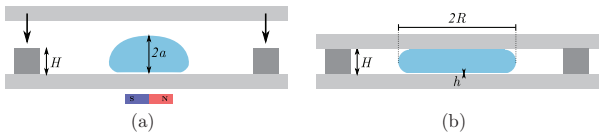

Fig. 1: (Colour on-line) (a) A large oxygen drop weakly trapped with a magnet is confined by an horizontal glass plate placed on spacers of thickness $H < 2a$. (b) When the drop is squeezed, two vapor films of thickness h prevent contact with the plates.

Experiments. –

Set-up. We use cryogenic liquids, in particular liquid oxygen, of Leidenfrost temperature lower than room temperature. Liquid oxygen is extracted from air, and ice crystals make it milky, which provides both a good contrast on a black background and a qualitative measurement of the thickness of liquid by absorbance. Liquid oxygen has a boiling temperature $T_b = 90\,\mathrm{K}$, a viscosity $\eta_l = 0.19\,\mathrm{mPa\cdot s}$, a density $\rho_l = 1140\,\mathrm{kg/m^3}$, a surface tension $\gamma = 13\,\mathrm{mN/m}$, and a capillary length $a = \sqrt{\frac{\gamma}{\rho_l g}} \approx 1.1\,\mathrm{mm}$. Since oxygen is paramagnetic, drops can be trapped with a magnet [12] in order to control their initial position. The magnetic field is weak, so that it does not modify the drop's shape and dynamics.

The substrates are 2 mm thick glass plates, kept at room temperature during experiments owing to their thermal capacity. After a puddle is formed and trapped by the magnet, another glass plate is placed on spacers of

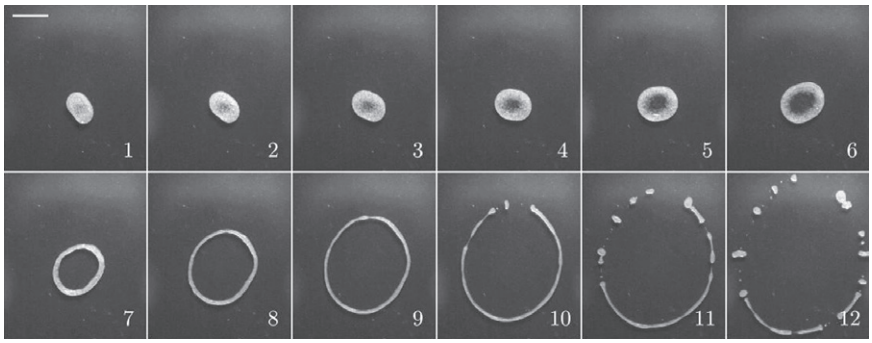

Fig. 2: Top view of the sequence of instabilities: i) the drop first slowly grows (images 1 to 6); ii) a hole nucleates in the center, which forms a ring; iii) the ring expands (images 7 to 9) before iv) breaking into droplets (images 10 to 12). Here we have $H = 0.6\,\mathrm{mm}$, the scale bar shows 1 cm and the interval between two snapshots is 14 ms.

height H, parallel to the first one. Since H is smaller than the thickness $2a$ of the puddle, this protocol confines the liquid between two "hot" surfaces, producing a vapor layer next to each plate, as sketched in fig. 1(b) and established by Celestini *et al.* [10]. The evolution of the drop is recorded from the top with a high-speed camera at 5000 frames per second. If the drop is small, it keeps a shape close to a disk, and its radius reduces due to evaporation on long timescales (several seconds) [10]. In contrast, a big drop is unstable and forms a fast growing ring, as shown in fig. 2. We repeated the experiments with liquid nitrogen ($T_b = 77\,\mathrm{K}$: $\eta_l = 0.16\,\mathrm{mPa\cdot s}$, $\rho_l = 807\,\mathrm{kg/m^3}$ and $\gamma = 9\,\mathrm{mN/m}$) and obtained similar results. While Raufaste *et al.* [11] studied drops at the onset of instability, we are able, thanks to our protocol, to observe the destabilization of drops much larger than the capillary length, with an initial diameter up to 12 mm for each H. The study of this sequence of instabilites, and more precisely the dynamics of opening of the ring, is the main topic of this article.

Ring formation and breaking. As shown in fig. 2 (movies `1-H0.4mm.avi`, `2-H0.6mm.avi`, `3-H0.6mm.avi`, `4-H1.0mm.avi` and `5-H1.3mm.avi` are available in the supplementary material[1]), the destabilization of the drop implies several steps:

A) First, the drop's apparent surface area slowly increases, and its center darkens, which corresponds to a thinning of the liquid (images 1–6).

B) Then, a faster phenomenon occurs: the thin central zone bursts in less than 10 ms, *i.e.*, less than the interval between frames 6 and 7 in fig. 2.

[1]Information about the movies: the movies present the evolution of various oxygen drops confined, from above. All movies are slowed down 125 times and their scale is given by the movie frame size. The corresponding spacing and scale of each movie are given by the following table.

Movie number	1	2	3	4	5
H (mm)	0.4	0.6	0.6	1.0	1.3
Frame size (cm)	2	5	4	5	3

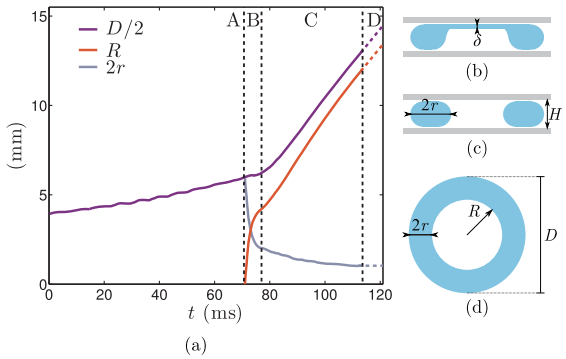

Fig. 3: (Colour on-line) (a) Example of drop temporal evolution: external radius $D/2 = R + 2r$ (purple), internal radius R (red), and width $2r$ (blue) ($H = 0.6\,\mathrm{mm}$). Dotted lines show limits between stages of the instability. Schematics: cross-section of the drop at the end of stage A (b), and at the beginning of stage C (c); top view of the ring (d).

C) At this stage, the drop adopts a ring shape. The radius of this ring quickly increases, while its width decreases due to volume conservation (images 7–9).

D) Finally, the expanding ring breaks into several fragments that expand further (images 10–12).

The instability of the ring is thus composed of several successive instabilities. Namely, we first observe the destabilization of the thickness of the drop (stage A), then the formation and expansion of the ring (stages B and C) and finally its fragmentation (stage D). The rings formed in stages B and C are described by their mean internal radius R, and by the average width $2r$ of the corona, as defined in fig. 3. These values can be estimated from two area measurements, using image analysis: the surface area Σ_{ext} of the ring (or drop, in stage A), and the surface area Σ_{int} of the hole when present (stages B and C). This leads to a total diameter $D = 2\sqrt{\Sigma_{ext}/\pi}$, an internal radius $R = \sqrt{\Sigma_{int}/\pi}$ and a ring width $2r = D/2 - R$. This allows us to distinguish the different stages of ring opening, as shown in fig. 3. Again, we first observe the opening of the central hole (stage B), a fast stage (less than 5 ms) during

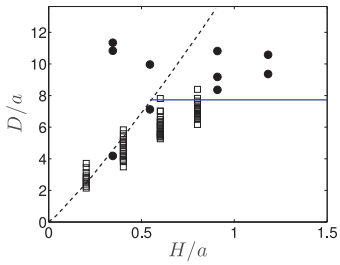

Fig. 4: (Colour on-line) Stability diagram of confined Leidenfrost drops, in terms of initial diameter D and confinement H normalized by the capillary length a. Circles represent the unstable drops studied throughout this work, and we only observe stable drops below both lines in this phase diagram. The blue solid line shows the unconfined limit $D_c = \sqrt{6}\pi a$ whereas the dashed curve is obtained from numerical integration [10]. Squares are threshold measurements extracted from Celestini *et al.* [10].

which the external radius $D/2$ remains constant. Meanwhile, the internal radius R grows at a constant velocity of $1.5 \pm 0.4\,\mathrm{m/s}$, before it slows down. Next, the ring expands (stage C): the external radius accelerates until it reaches a constant velocity. Simultaneously, the internal radius grows at approximately the same velocity, while the width decreases due to volume conservation. This stage lasts until the ring breaks, after which the system keeps on growing by inertia (stage D).

Instability analysis. – We now analyze the sequence of instabilities following chronological order.

A): Thinning stage. When a drop is confined between two parallel plates, the liquid first migrates toward the periphery, decreasing the central thickness (images 1–6 in fig. 2). When the drop is moderately confined ($H \approx a$), the mechanism is similar to the instability observed with a Leidenfrost puddle, where the light vapor film can be unstable. As described by Taylor for hanging films [13], the instability occurs when the system is large enough: then the vapor pocket rises and eventually forms a chimney across the drop [7,10]. This chimney releases the vapor, and the hole closes by surface tension. More recently, it was shown that holes appear above a minimum radius $D_c = \sqrt{6}\pi a \approx 7.7a$, where a is the capillary length [7,8]. For liquid oxygen with $a \approx 1.1\,\mathrm{mm}$, we expect $D_c \approx 8.3\,\mathrm{mm}$, which compares to the minimum size observed for unstable confined drops, as shown in fig. 4. We can estimate the characteristic time this case as the time needed for the destabilization of a vapor film of thickness $h \approx 100\,\mu\mathrm{m}$ and viscosity $\eta_v \approx 1.4\ 10^{-5}\,\mathrm{Pa \cdot s}$. Assuming a Poiseuille flow for the vapor, this time scales as $12\gamma\eta_v/\rho_l^2 g^2 h^3$ [14], approximately 10 ms here, a value comparable to the timescale of "spreading" in fig. 2.

We also noticed that the threshold size decreases for $H/a \leq 0.5$ (fig. 4), in good agreement with the results obtained numerically and experimentally by Celestini *et al.* [10]. In this case of highly confined drops, the origin of the instability is different: pressure rises in the gas film due to the radial lubrication flow from evaporation. It leads to inhomogeneous films, thinner at the center of the drop [10].

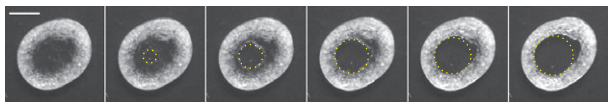

Fig. 5: (Colour on-line) Image sequence of the opening of the central film (stage B) underlined by a dotted circle, for $H = 0.6\,\mathrm{mm}$. The scale bar shows 5 mm and the time interval between snapshots is 0.6 ms.

B): Ring opening. Above D_c, a vapor cavity grows below the drop, and the resulting liquid film eventually breaks and bursts (stage B). This explosion is illustrated by the image sequence in fig. 5, where the hole in the film is underlined by dotted circles.

As a remark, we can notice that a similar expansion mechanism is observed in stages A and C, yet at very different velocities $\dot{R}$ (fig. 3(a)). The liquid repartition at the end of stage A mostly differs from stage B by a liquid film of surface area $2\pi R^2$ (figs. 3(b) and (c)). Since it costs energy to stretch this film, it makes the ring difficult to expand, compared to the ring in stage C: if there is no film at the center of the ring, the surface tension resistance to expansion becomes much smaller, by a factor scaling as $\frac{R}{H} \approx 10$. This explains why the fast expansion (phase C) is triggered by the bursting of the central liquid film (phase B).

Stage B begins with a rapid increase of the internal radius R at constant velocity while the external radius remains constant (as shown in fig. 3). The bursting velocity is high, and it barely changes with drop volume or confinement: our measurements yield $\dot{R} = 1.5 \pm 0.4\,\mathrm{m/s}$, with no visible correlation with D or H. This behavior is similar to the one following the bursting of a soap film of thickness δ, studied by Culick [15] who predicted a bursting velocity:

$$\dot{R} = \sqrt{\frac{2\gamma}{\rho_l \delta}}. \qquad (1)$$

Using eq. (1), we can estimate δ around $10\,\mu\mathrm{m}$. During the free fall of large drops, the air flow also leads to the formation of liquid sheets [16]. Those films also break around $10\,\mu\mathrm{m}$. For comparison, soap films are often thinner (typically $1\,\mu\mathrm{m}$) yet they are stabilized by surfactants.

We considered the film undisturbed away from the rim, which explains that the external radius of the drop remains constant in this stage. Moreover, the rim is much lighter than the drop: at the beginning of stage B, the volume of the central film scales as δR^2, a small fraction $\delta R/rH \sim 1\%$ of the volume of the drop. Finally, the film becomes thicker in the vicinity of the ring, which explains that the opening velocity decreases at the end of stage

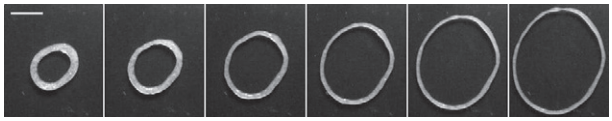

Fig. 6: Image sequence of an expanding ring (stage C). We have $H = 0.6\,\mathrm{mm}$, the scale bar corresponds to 1 cm and the time interval between photos is 7.2 ms.

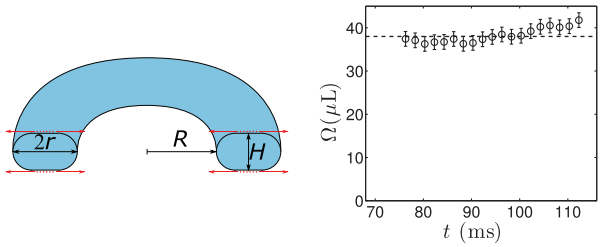

(a) (b)

Fig. 7: (Colour on-line) (a) Red arrows show the vapor flow inward or outward, below and above the liquid: due to confinement, vapor going inside the ring cannot escape and triggers expansion. (b) Volume $\Omega = 2\pi(R+r)[(2r-H)H + \pi H^2/4]$ *vs.* time t during stage C, for the experimental data of fig. 3. The mean value, $\Omega = 38\,\mu\mathrm{L}$, is plotted with a dotted line.

B. Unlike Raufaste *et al.* [11], we do not find any correlation between the opening velocity and the confinement. However, the decrease of the velocity is similar to the one they observed and predicted using a refined version of this model assuming a linear profile of thickness instead of a uniform film.

C): Expanding ring. After its formation, the ring expands, as shown in fig. 6: its radius R increases and its width consequently decreases. This expansion of typical velocity of 0.1 m/s is much faster than the initial growth of the drop.

Several physical mechanisms can explain the resistance to expansion. Firstly, stretching the ring produces an internal flow with viscous dissipation. Comparing the radial inertia of the ring $\rho_l \dot{R}^2$ to the viscous dissipation $\eta_l \dot{r} R/r^2 \sim \eta_l \dot{R}/r$ leads to a Reynolds number $Re = \rho_l \dot{R} r/\eta_l \approx 10^3$, which allows us to neglect viscosity inside the ring. Secondly, surface tension could stop expansion and even close the ring, as observed with a liquid ring on a bath [17] or in a standard Leidenfrost state [18]. The Laplace pressure difference between inside and outside is $\gamma(\frac{1}{R+r} + \frac{1}{R})$, hence scaling as γ/R for large rings ($r \ll R$). Comparing inertia to surface tension yields a Weber number $We = \rho_l \dot{R}^2 R/\gamma$, always larger than 100 for $R \geq 1\,\mathrm{cm}$: surface tension effects are smaller than inertia. Raufaste *et al.* also studied the expansion dynamics and claimed that it is driven by the inertia acquired by liquid during the previous stage [11]. They measured a velocity scaling as $\sqrt{\gamma/\rho H}$. Instead of a constant velocity, we measure a small yet appreciable increase of velocity at the beginning of stage C, and our typical velocities decrease more strongly with H. Moreover, in our case, as already mentioned, the film is much lighter than the drop. Finally, inertia alone cannot be responsible for the opening of the ring: holes are also formed in standard Leidenfrost puddles following processes similar to stage A and B, but they close due to surface tension. This underlines the key role of confinement, and suggests that expansion is driven by the gas flowing to the central hole instead of inertia.

Since the glass temperature is much higher than the boiling point of the liquid, vapor is produced and part of it accumulates in the central pocket formed during the preceding stages. The variation of the product of the internal pressure by the volume of the pocket $\pi R^2 H$ is related to the injected mass by the ideal gas law. Assuming that the difference between the pressure in the pocket and the external one is constant, we deduce that the change of volume of the central pocket due to evaporation drives the motion. We thus focus on the opening law $R(t)$, for $r \ll R$. On the other hand, the ring volume $\Omega = 2\pi(R+r)[2rH + (\pi/4-1)H^2] \sim rRH$ is assumed to be constant during the short timescale of experiments, which lasts approximately 100 ms, much smaller than the characteristic timescale of evaporation, typically 10 s. This is consistent with the evolution of Ω presented in fig. 7. As usually assumed in a Leidenfrost state [7,10], the thermal diffusion through a vapor film of thickness h controls the evaporation of the drop, which yields the mass rate of evaporation:

$$\dot{m} \sim \lambda \Delta T R r/hL, \tag{2}$$

where $\Delta T \approx 200\,^\circ\mathrm{C}$ is the difference of temperature between the drop and its substrate, $L = 210\,\mathrm{kJ/kg}$ the latent heat of oxygen and $\lambda = 0.018\,\mathrm{W \cdot m^{-1} \cdot K^{-1}}$ the thermal conductivity in the gas. Conservation of mass for vapor gives $\dot{m} \sim \rho_v R h u$, where $\rho_v = 2.0\,\mathrm{kg/m^3}$ is the vapor density and u its characteristic velocity. In a confined Leidenfrost state, the pressure in the drop is fixed by the spacing between the plates, and scales as γ/H for $h \ll H \ll a$. The gas flow thus results from a pressure gradient γ/Hr: assuming that the velocity of gas is given by a Poiseuille flow, we deduce $u \sim h^2\gamma/\eta_v H r$, where $\eta_v = 14\,\mu\mathrm{Pa \cdot s}$ is the vapor viscosity. From previous equations, we find that the thickness of the gas layer is fixed by the width r of the ring and a characteristic length $b = \sqrt{\frac{H}{\gamma}\frac{\eta_v}{\rho_v}\frac{\lambda \Delta T}{L}}$, according to

$$h \sim \sqrt{br}. \tag{3}$$

If a constant fraction of the produced vapor feeds the gas pocket, its mass grows as $\dot{m} \sim \rho_v H R \dot{R}$, driving the expansion of the ring. Together with these equations, we express the liquid volume conservation, which yields the following differential equation, for $r \ll R$:

$$R^{1/2}\dot{R} \sim \frac{\lambda \Delta T}{\rho_v L}\sqrt{\frac{\Omega}{bH^3}}, \tag{4}$$

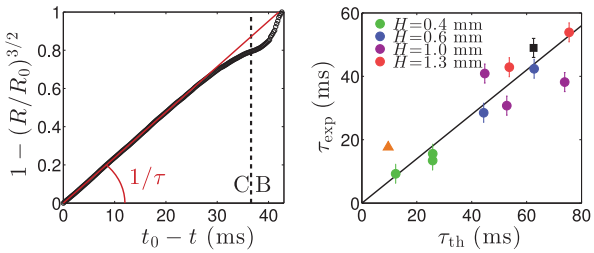

(a) (b)

Fig. 8: (Colour on-line) (a) From the data displayed in fig. 3, we plot $1-(R/R_0)^{3/2}$ as a function of $t_0 - t$, for $t_0 = 113$ ms. The expansion of the ring (stage C) is asymptotically well described by eq. (5). The characteristic time τ can be deduced from the linear fit (in red) (here, $\tau_{\rm exp} = 42$ ms). (b) $\tau_{\rm exp}$ as a function of the theoretical value $\tau_{\rm th}$ expected from eq. (5), for liquid oxygen and various spacings H (circles). The best linear fit gives 0.7 for the slope. The black square corresponds to an experiment with liquid nitrogen and $H \approx 1.0$ mm while the orange triangle is evaluated from data by Raufaste *et al.* [11] on a water drop, with $H \approx 1$ mm and $\Omega \approx 85\,\mu$L.

where the right-hand side is constant. Denoting $R(t = t_0) = R_0$, we solve this equation for $R(t)$ and find

$$R(t) = R_0 \left(1 + \frac{t - t_0}{\tau}\right)^{2/3} \quad \text{with } \tau \sim \frac{\rho_v L}{\lambda \Delta T}\sqrt{\frac{bH^3R_0^3}{\Omega}}. \tag{5}$$

For a given drop, the horizontal surface of the ring rR is fixed, and from $\Omega \sim rRH$ and $b \propto H^{1/2}$, we deduce $\tau \propto H^{5/4}$: the smaller the spacing H, the faster the expansion. In a general case, τ depends on both H and Ω (different for each experiment), and one also needs to specify t_0 (or R_0) in order to compare eq. (5) to data. It is tempting to choose the beginning of stage C, but it is hard to determine precisely this time in experiments. Since eq. (4) shows that the dynamics does not depend on R_0, we rather choose for R_0 the last available data point, that is, the instant before the opening of the ring (end of stage C), which also satisfies the limit $r \ll R$. In fig. 8(a), we plot $1-(R/R_0)^{3/2}$ as a function of $t_0 - t$, and we obtain, as expected, a line passing through the origin. From the slope of this line, we deduce the value of τ, and present in fig. 8(b) such measurements, showing a good agreement with the value predicted by eq. (5). For this estimation, we used the physical properties of gaseous oxygen at $-80\,^\circ$C, the mean temperature between boiling point and glass temperature ($20\,^\circ$C). From this plot, the numerical factor in the expression of τ (eq. (5)) is found to be 0.7. The agreement between model and experiments remains good for a confined drop of liquid nitrogen (black square in fig. 8(b)). For comparison with an inertial model, the typical velocity R_0/τ does not vary as $H^{-1/2}$ but is rather coherent to the dependence as $H^{-5/4}$ expected from our model. On the other hand, the temporal evolution reported by Raufaste *et al.* [11] for a water drop

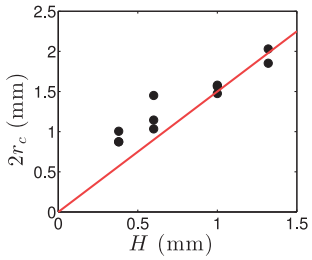

Fig. 9: (Colour on-line) Ring width $2r_c$ at the first rupture (beginning of stage D) *vs.* the spacing H. The fitting line's slope is 1.5.

is also in good agreement with our model: applying the method described above on their data, we obtain a plot similar to fig. 8(a) using $R_0 \approx 5.8$ mm for $t_0 \approx 20$ ms. The linear fit gives the value of $\tau_{exp} \approx 18$ ms (orange triangle in fig. 8(b)).

D): Fragmentation of the ring. As the ring expands, its width decreases until the liquid thread becomes unstable and breaks up in several droplets (fig. 2). This is a classical Rayleigh-Plateau instability, initially studied for cylinders [19,20], but also valid for a liquid torus provided it is large enough [17,21–23]. A condition for torus fragmentation is $(R + r)/r > 2$ [17,24], corresponding to $r < R$, a condition always fulfilled in our experiments. Despite the fragmentation of the liquid thread, the expansion of the liquid continues, owing to the inertia acquired in previous stages and to the low friction inherent to the Leidenfrost state.

We focus on the first rupture of the ring, and measure the mean width $2r_c$ at which it breaks. Figure 9 shows that rupture occurs when the width is proportional to the thickness of the ring, fixed by the confinement spacing H. More precisely, we found $2r_c \approx 1.5H$, close to the situation where the section is circular and the liquid unconfined. Indeed, the Rayleigh-Plateau instability might not develop when liquid is squeezed, as reported for other kinds of confinement [25]. At small thickness ($H \leq 0.6$ mm), the critical width is higher than this linear law ($2r_c > 1.5H$). Early ruptures occur for thin threads of fluctuating width, which can locally produce fragmentation. Finally, with this scaling, we can refine the law on τ since we chose R_0 at the onset of stage D: assuming $\Omega \sim R_0H^2$, we deduce $\tau \propto H^{-5/4}\Omega$, in agreement with the observed influence of the volume.

The driving mechanism of fragmentation is surface tension, and we can wonder whether the resistance is viscous or inertial. We consider that the thread is locally cylindrical ($R \gg r$) and thus neglect the effect of the radius of curvature R on the fragmentation. The relevant physical properties for a viscous instability are the thread radius r, the surface tension γ and the liquid viscosity η_l, with a corresponding viscous characteristic time $\tau_v \sim \eta_l r/\gamma$, typically 10 μs for our parameters. When inertia resists the instability, the associated timescale becomes

$\tau_i \sim \sqrt{\rho_l r^3/\gamma}$, whose value typically is 10 ms. Since $\tau_v \ll \tau_i$, kinetics is set by inertia. It is worth noticing in fig. 2 that the time interval between two consecutive ruptures is indeed comparable to this inertial characteristic time.

Finally, we can compare this timescale to the typical time needed to change the ring radius, that scales as $r/\dot{r} \sim R/\dot{R} \sim \tau$. In our experiments $\tau > \tau_i$: the fragmentation is mostly unaffected by the expansion of the ring, but studying the coupled effects would be interesting.

Conclusion. – The instability of large Leidenfrost drops confined between two hot plates is usually initiated by a Rayleigh-Taylor instability, as reported for regular Leidenfrost puddles. It gathers the liquid on the edges of the drop, leaving at the center a liquid film that bursts when its thickness is typically 10 μm. A liquid ring forms and grows due to its evaporation: the gas, trapped by confinement, drives the expansion, decreasing the ring's width. When this width compares to the spacing, the resulting torus is subjected to the Plateau-Rayleigh instability, so that it decays into multiple droplets.

In addition to setting the maximum size of a confined Leidenfrost drop, this sequence of events is a beautiful illustration of several classical instabilities of liquid interfaces arising here from the flow produced by evaporation. Confinement is critical for triggering them: if the gas can easily flow away (*e.g.*, on a single plane), a Leidenfrost ring is also unstable [18] but the other way around, since it spontaneously closes, driven by surface tension!

REFERENCES

[1] Celestini F., Frisch T. and Pomeau Y., *Soft Matter*, **9** (2013) 9535.
[2] Perrard S., Couder Y., Fort E. and Limat L., *EPL*, **100** (2012) 54006.
[3] del Cerro D. A., Marín Á. G., Römer G. R. B. E., Pathiraj B., Lohse D. and Huis in't Veld A. J., *Langmuir*, **28** (2012) 15106.
[4] Vakarelski I. U., Patankar N. A., Marston J. O., Chan D. Y. C. and Thoroddsen S. T., *Nature*, **489** (2012) 274.
[5] Weickgenannt C. M., Zhang Y., Sinha-Ray S., Roisman I. V., Gambaryan-Roisman T., Tropea C. and Yarin A. L., *Phys. Rev. E*, **84** (2011) 036310.
[6] Linke H., Alemán B. J., Melling L. D., Taormina M. J., Francis M. J., Dow-Hygelund C. C., Narayanan V., Taylor R. P. and Stout A., *Phys. Rev. Lett.*, **96** (2006) 154502.
[7] Biance A.-L., Clanet C. and Quéré D., *Phys. Fluids*, **15** (2003) 1632.
[8] Snoeijer J. H., Brunet P. and Eggers J., *Phys. Rev. E*, **79** (2009) 036307.
[9] Burton J. C., Sharpe A. L., van der Veen R. C. A., Franco A. and Nagel S. R., *Phys. Rev. Lett.*, **109** (2012) 074301.
[10] Celestini F., Frisch T., Cohen A., Raufaste C., Duchemin L. and Pomeau Y., *Phys. Fluids*, **26** (2014) 032103.
[11] Raufaste C., Celestini F., Barzyk A. and Frisch T., *Phys. Fluids*, **27** (2015) 031704.
[12] Piroird K., Clanet C. and Quéré D., *Phys. Rev. E*, **85** (2012) 056311.
[13] Taylor G. I., *Proc. R. Soc. London, Ser. A*, **201** (1950) 192.
[14] De Gennes P.-G., Brochard-Wyart F. and Quéré D., *Capillarity and Wetting Phenomena: Drops, Bubbles, Pearls, Waves* (Springer) 2004.
[15] Culick F. E. C., *J. Appl. Phys.*, **31** (1960) 1128.
[16] Clift R., Grace J. R. and Weber M. E., *Bubbles, Drops and Particles* (Academic Press) 1978.
[17] Pairam E. and Fernández-Nieves A., *Phys. Rev. Lett.*, **102** (2009) 234501.
[18] Darbois Texier B., Piroird K., Quéré D. and Clanet C., *J. Fluid Mech.*, **717** (2013) R3.
[19] Plateau J., *Statique expérimentale et théorique des liquides soumis aux seules forces moléculaires* (Gauthier-Villars) 1873.
[20] Lord Rayleigh, *Proc. London Math. Soc.*, **10** (1879) 4.
[21] McGraw J. D., Li J., Tran D. L., Shi A.-C. and Dalnoki-Veress K., *Soft Matter*, **6** (2010) 1258.
[22] Yao Z. and Bowick M. J., *Eur. Phys. J. E*, **34** (2011) 1.
[23] Mehrabian H. and Feng J. J., *J. Fluid Mech.*, **717** (2013) 281.
[24] Jensen O. E., *J. Fluid Mech.*, **331** (1997) 373.
[25] Gau H., Herminghaus S., Lenz P. and Lipowsky R., *Science*, **283** (1999) 46.